Quaternary Science Reviews 281 (2022) 107420

Contents lists available at ScienceDirect

Quaternary Science Reviews

journal homepage: www.elsevier.com/locate/quascirev

Asian-Australian monsoon evolution over the last millennium linked to ENSO in composite stalagmite $\delta^{18}O$ records

Jian Zhang [a, b, c, 1], Ming-Qiang Liang [d, 1], Ting-Yong Li [a, *], Chao-Jun Chen [c], Jun-Yun Li [c]

[a] Yunnan Key Laboratory of Plateau Geographical Processes & Environmental Changes, Faculty of Geography, Yunnan Normal University, Kunming, 650500, China
[b] Environnements et Paléoenvironnements Océaniques et Continentaux (EPOC), UMR CNRS, 5805, Université de Bordeaux, Pessac, 33600, France
[c] Chongqing Key Laboratory of Karst Environment, School of Geographical Sciences, Southwest University, Chongqing, 400715, China
[d] Department of Geosciences, National Taiwan University, Taipei, 10617, Taiwan, China

ARTICLE INFO

Article history:
Received 23 November 2021
Received in revised form
6 February 2022
Accepted 9 February 2022
Available online xxx

Handling Editor: Qiuzhen Yin

Keywords:
The past millennium
Asian-Australian monsoon
Stalagmite $\delta^{18}O$
Integrated research
ENSO

ABSTRACT

The Asian-Australian monsoon (AAM) system distinctly influences global climate. However, the linkage between ENSO (El Niño–Southern Oscillation) and AAM is still poorly understood over the last millennium. Here, we combined stalagmite $\delta^{18}O$ ($\delta^{18}O_s$) records with exceptionally high-resolution and high-precision chronologies to demonstrate a tight remote coupling between AAM and tropical ocean hydrology on the multi-year, decadal, and centennial timescales. Our results reveal that **(1)** There is a significant negative correlation between the multi-year weighted average precipitation $\delta^{18}O$ ($\delta^{18}O_{aw}$) from the AAM and Southern Oscillation Index (SOI), providing a modern analogous coupling for linking stalagmite $\delta^{18}O$ ($\delta^{18}O_s$) and ENSO over the past 100 years. **(2)** Over the last millennium, the integrated $\delta^{18}O_s$ record exhibit positive excursions during the Little Ice Age (LIA), marked by a tendency for more El Niño-like state conditions in the tropical Pacific, which is consistent in SST-gradient ENSO reconstruction but different to precipitation reconstruction. **(3)** Wavelet and power spectrum analysis for the integrated $\delta^{18}O_s$ record in the AAM region show that there is a significant multi-year periodicity (2.2, 2.8, 3.5, 4.6 yr), conceding with the ENSO cycle (2–7 yr), whereas, some multi-decadal and centennial cycles (10.1, 17, 28.6, 52.7, 143 yr) are significant too. We provide evidence from instrumental and paleocliamte datasets (GNIP and NOAA) and propose a possible "circulation effect" mechanism responsible for variations of $\delta^{18}O_s$ in the East Asian Monsoon (EAM) and Australian Monsoon (AM) region over the last millennium.

1. Introduction

The El Niño-Southern Oscillation (ENSO) (Table S1) influences interannual climate variability across huge swaths of the globe and can lead to large-scale atmospheric climate variability. The inversely correlated Southern Oscillation Index (SOI) and Sea-Surface Temperature Anomaly (SSTA) index in the Niño 3.4 region (5° N-5° S, 170° W-120° W) are common benchmarks of ENSO intensity (Ropelewski, and Jones, 1987; Trenberth, 1997). El Niño and La Niña events regulate the climate variability over the vast majority of the Pacific region and, through the atmosphere-ocean bridge (e.g., Kelvin and Rossby waves), influence climate worldwide (Liu and Alexander, 2007; Alexander et al., 2010).

Stalagmite oxygen-isotope ($\delta^{18}O_s$) records have been widely used to characterize Asian-Australian Monsoon (AAM) variations and further indicate local to regional precipitation change in the AAM region over the last millennium (Hu et al., 2008; Zhang et al., 2008; Berkelhammer et al., 2010; Zhao et al., 2015; Denniston et al., 2016). However, many studies have contended that a direct link is somewhat controversial between $\delta^{18}O_s$ records and local–regional precipitation anomalies (Tan, 2014, 2016). For example, the explanations, elucidating the amount effect, emphasize large-scale atmospheric processes, which modulate the isotopic fractionation of water vapor during the migration from upstream to downstream regions (Bowen et al., 2019). More specifically, the upstream precipitation and convective activity can isotopically deplete lower-tropospheric water vapor prior to rainout over the cave sites (Cai et al., 2017). However, based on the Rayleigh distillation equation (Rayleigh, 1896), changes in the atmospheric-oceanic circulation

* Corresponding author.
E-mail addresses: jian.zhang@u-bordeaux.fr (J. Zhang), lmq041@gmail.com (M.-Q. Liang), cdlity@163.com (T.-Y. Li).
[1] The first authors: Jian Zhang and Ming-Qiang Liang.

https://doi.org/10.1016/j.quascirev.2022.107420
0277-3791/

directly or indirectly affect the variation in the ratio of water vapor originating from distant oceans (becoming depleted in ^{18}O) and local ocean (relatively enriched in ^{18}O) to an observed site, resulting in the fluctuation of the precipitation oxygen-isotope ($\delta^{18}O_p$) at this site (Tan, 2014, 2016). In light of the above theory, the "circulation effect" proposed by Tan (2014, 2016) suggests that $\delta^{18}O_p$ and $\delta^{18}O_s$ in EASM region might be affected by different moisture sources and trajectories controlled by variations in atmospheric–oceanic circulation modes, which are related to ENSO (Tan, 2014, 2016; Zhang et al., 2019).

In addition, by combining precisely dated stalagmite records from southern China and northern Australia, Denniston et al. (2013) revealed an unidentified coherence between the austral and boreal summer monsoon, which is attributed to the local response caused by the atmosphere's meridional circulation changes in Australian Monsoon (AM) (Denniston et al., 2013, 2016). However, the existing studies of $\delta^{18}O_s$ as a proxy of circulation modes are limited to their respective sampling regions, lacking a comprehensive portrait that more coherently captures the ENSO signal from $\delta^{18}O_s$ across the entirety of AAM realms (Zhang and Li, 2018).

There are a series of multi-proxies ENSO reconstructions from previous studies, including tree rings, ice cores, corals (Gergis and Fowler, 2009; McGregor et al., 2010; Emile-Geay et al., 2013; Liu et al., 2017). However, the reconstructions of ENSO across the last millennium have not yet yielded a consistent picture of the mean state of the tropical Pacific or temporal changes of ENSO variations, whether from paleoclimate proxies (Mann et al., 2000; Cobb et al., 2003; Conroy et al., 2010; Yan et al., 2011a, 2011b; Chen et al., 2015; Tan, 2016) or climate model simulations (Mann et al., 2005; Man et al., 2011, Table S2). Although some reconstructions based on tree rings and coral growth bands potentially capture variabilities at the annual resolution, several disputes over the interpretation of these reconstructions, such as insufficient record length and the climatic significance of these proxies (Cobb et al., 2003; Liu et al., 2017), still limit our understanding of long-term ENSO variation and the role of external drivers during the past millennium.

Herein, we, combining high-resolution stalagmite records with ultra-precise U–Th chronologies, attempt to resolve questions that arise from other proxies, validating our interpretation against recent $\delta^{18}O_p$ in the AAM region from GNIP and NOAA datasets. Our new understanding in this study can be summarized as follows: **(1)** a strong link between $\delta^{18}O_p$ and SOI is observed in the AAM region; **(2)** a long-term PCA (Principal Component Analysis) $\delta^{18}O_s$ sequence from the AAM region is linked with the ENSO variability over the past millennium, with a robust validation based on instrumental ENSO measurements.

2. Study area

The AAM region consists of three monsoon subsystems, namely the East Asian Monsoon (EAM), Indian Monsoon (IM), and Australian Monsoon (AM) (Fig. 1A and 1B; Table S1; Ding and Chan, 2005). The correlation between surface-air temperature anomaly and SST anomalies in the eastern and central equatorial Pacific (ECEP) was calculated in Fig. 1B, combining the data for all calendar months during the El Niño years over the period 1979–2006 C.E.

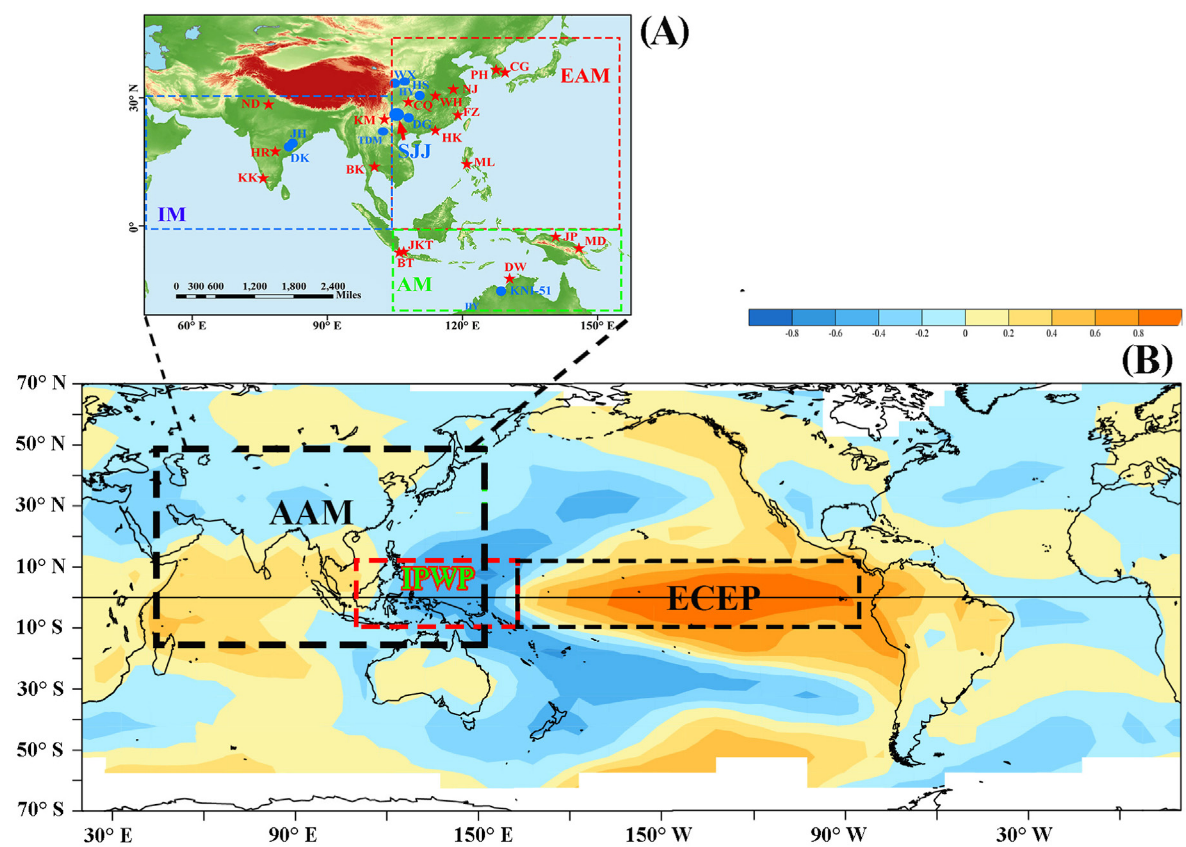

Fig. 1. **(A)** Distribution of GNIP meteorological stations (red stars) and stalagmite records (blue dots) in this study. For each site, detailed geographical information was listed in Tables S2 & S3. **(B)** Typical El Niño years' sea-surface temperature (SST) anomalies in Niño 3.4 zone correlated with global surface temperature for all calendar months during the period 1979–2006 (C.E.) (data source: http://research.jisao.washington.edu/data_sets/er-ghcn/). Abbreviations in the diagram are explained in Table S1. (For interpretation of the references to colour in this figure legend, the reader is referred to the Web version of this article.)

Detailed geographic information for meteorological stations is summarized in Table S3. All geographic information for stalagmite records is summarized in Table S4. The hydroclimate of the IM region is characterized by a "relatively coherent single moisture source" transported from the Indian Ocean (Pathak et al., 2017; Zhang and Li, 2018). The EAM and the AM regions are dominated by "composite moisture sources" from the Western Pacific and the Indian Ocean (Liu et al., 2014), and the boundary between the EAM and IM region is conventionally divided at 105°E (Wang et al., 2003).

3. Method

Our $\delta^{18}O_s$ integration is based on the following logical reasoning. First, we identified a strong link between $\delta^{18}O_p$ and SOI in the AAM region, providing modern observational evidence for the use of $\delta^{18}O_s$ to constrain ENSO variability. Second, we contended that $\delta^{18}O_s$ inherits the isotopic composition of atmospheric precipitation (Lachniet, 2009; Pape et al., 2010; Li et al., 2011a; Genty et al., 2014; Chen and Li, 2018; Sun et al., 2018) with a similar signal across the AAM region; therefore, the respective $\delta^{18}O_s$ series in different regions can be used to link with ENSO, and also reveal that strong links existed between the AAM and ENSO systems over the past millennium. Finally, the reliability of the link between the integrated $\delta^{18}O_s$ with high-resolution and ENSO is validated by the well-constrained instrumental SOI data over the past 100 years.

We analyze twelve published $\delta^{18}O_s$ records from the AAM region (Table S4). These records are chosen on the basis that they have high-resolution with accurate dating and overlap over the last millennium as long as possible (Table S4). To facilitate data analysis and integration, the original stalagmite records are linearly interpolated to a unified chronology of annual resolution, for which we obtain corresponding $\delta^{18}O_s$ value. To minimize the impacts of different absolute values of $\delta^{18}O_s$ across the AAM region, a Z-scores method is employed to convert the absolute $\delta^{18}O_s$ value into a unified measurement for the inter-site comparison, without changing the temporal signal of each series. A Principal Component Analysis (PCA), the multivariate statistical technique was applied in their scientific disciplines (Abdi et al., 2010), and extracted the dominant modes of variability and explore important factors affecting the $\delta^{18}O_s$ over the last millennium in the AAM region. In addition, becasue of the different temporal coverage of each stalagmite, we use a partitioning synthesis approach to synthesize the final curve based on the principle of covering more stalagmites and the longer period. Detailed calculation steps and formula refer to the method from Supplementary materials.

4. Results

4.1. Relationships between $\delta^{18}O_p$, rainfall amount, and ENSO index

The $\delta^{18}O_p$ is the source of $\delta^{18}O_s$, so we first analyze the variation characteristics of $\delta^{18}O_p$ in the AAM region. There is a significant negative relationship between monthly $\delta^{18}O_p$ and precipitation amount for these meteorological sites in the AAM region ($p < 0.05$ or $p < 0.01$) (Table S5), indicating a statistically robust correlation on a seasonal timescale (Dansgaard, 1964). However, no inter-annual correlation ($p > 0.1$) (Table S6) is observed between the annal weighted precipitation $\delta^{18}O$ ($\delta^{18}O_{aw}$) and local annual precipitation (AP) at meteorological stations from the EAM and AM regions, with the exception of positive correlations observed in Cheongju (CG), Chongqing (CQ), Jakarta (JKT), and Wuhan (WH) stations (Table S6). This positive correlation is contrary to the "amount effect", indicating that the $\delta^{18}O_{aw}$ in these regions affected by composite moisture sources does not reflect changes in local precipitation amount on inter-annual timescales. However, it is worth noting that at the three sites in the IM region (Bangkok (BK), Kozhikode (KK), and New Delhi (ND)), a significant negative correlation is presented between $\delta^{18}O_{aw}$ and local annual precipitation on the inter-annual timescales (Table S6).

Due to the discontinuous limitation of some GNIP site data, we only analyze the three longest and relatively continuous datasets in the meteorological stations from Hong Kong (HK), Bangkok (BK), and Darwin (DW) to represent EAM, IM, and AM region, respectively. (Fig. 2A, 2B, 2C; Zhang and Li, 2018). We observe that there are significant negative correlations between the $\delta^{18}O_{aw}$ and SOI in the station of HK (EAM region) ($p < 0.01$) (Tan, 2014), DW (AM region) ($p < 0.01$) (Liu et al., 2010, Fig. 2A and 2B), and BK station (IM region) ($p < 0.05$) (Fig. 2C), supporting the hypothesis that ENSO footprint can strongly influence the oxygen-isotope records

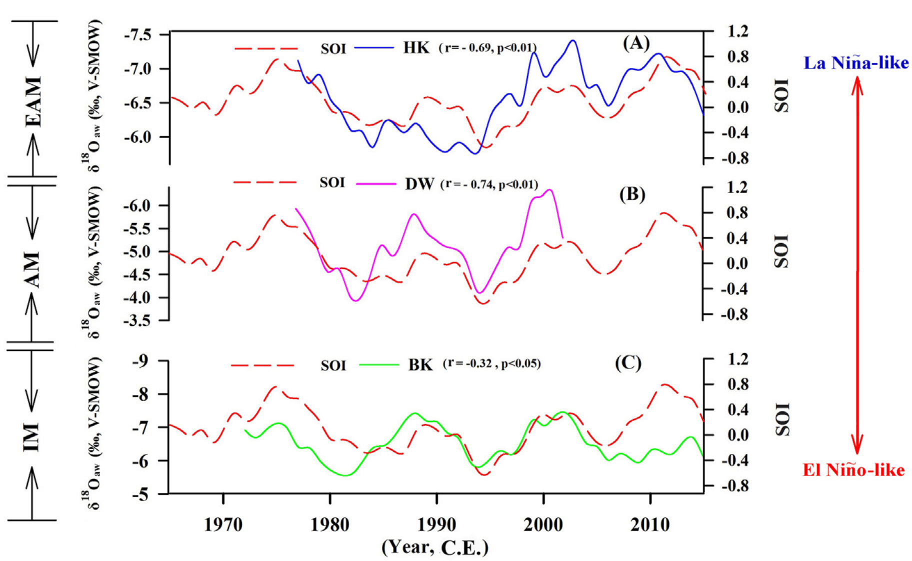

Fig. 2. Comparison between $\delta^{18}O_{aw}$ and SOI in the AAM region. **(A)** SOI vs. $\delta^{18}O_{aw}$ of Hong Kong (HK) in the EAM region. **(B)** SOI vs. $\delta^{18}O_{aw}$ of Darwin (DW) in the AM region. **(C)** SOI vs. $\delta^{18}O_{aw}$ of Bangkok (BK) in the IM region. To exhibit the interannual signals in $\delta^{18}O_{aw}$ and SOI, the raw data have been processed by a 5-year moving average. In annual to decadal timescales, there are significant negative correlations between $\delta^{18}O_{aw}$ and SOI over the whole AAM region.

in the AAM region.

4.2. Trend of stalagmite $\delta^{18}O$ records over the past 1 ka in the AAM region

Several published high-resolution stalagmite records in the AAM region cover the past millennium (Sinha et al., 2007; Hu et al., 2008; Zhang et al., 2008; Berkelhammer et al., 2010; Tan et al., 2011; Zhao et al., 2015; Denniston et al., 2016; Wang et al., 2019; Li et al., 2021; Table S4). To reduce the uncertainty in exploring the relationship between ENSO and monsoon, these records with high-resolution $\delta^{18}O_s$ series and accurate chronologies have been comprehensively analyzed in this study.

These stalagmite records were processed onto a common time series by the Z-scores conversion and linear interpolation method. The main findings of this compilation are as follows: **(1)** all $\delta^{18}O_s$ records exhibit similar trends, and the structure of $\delta^{18}O_s$ variations in the AAM region is analogous especially during the Little Ice Age (LIA) (Fig. 3A, 3B, 3C); **(2)** the trend of $\delta^{18}O_s$ records is generally consistent during the LIA, with no distinguishable interhemispheric see-saw pattern (Zhao et al., 2015, Fig. 3). The overall trend of $\delta^{18}O_s$ records over the past millennium in the AAM region is generally consistent on multi-decadal and centennial timescales, indicating that the change of $\delta^{18}O_s$ may be controlled by a common climatic mechanism in the AAM region (Fig. 3).

4.3. The PCA $\delta^{18}O_s$ integration and verification linked to ENSO

We used 12 high-resolution terrestrial stalagmite proxy records from EAM, IM, and AM to extract the main characteristics of stalagmite variability over the past 100 years and 1000 years (Fig. 4A; 4C), validated by the instrumented SOI index (Fig. 4B). Comparing the instrumental SOI with the reconstructed $\delta^{18}O_s$ variation, a significant inverse correlation ($r = -0.54$, $p < 0.01$) is observed during the period 1900–2000 (C.E.) (Fig. 4B). The linear variation trend also decreases in the instrumental SOI and Z-scores $\delta^{18}O_s$ on the inter-decadal timescale (Fig. 4B), which is consistent with a negative relationship between $\delta^{18}O_{aw}$ and SOI (Fig. 2), exhibiting a transition from a La Niña-like state to an El Niño-like state (Fig. 4B) during the late-1970s. Wavelet and power spectrum analyses for the integrated $\delta^{18}O_s$ record of AAM stalagmites over the past 100 years also show that there are significant periodicities (e.g., 2.2, 2.8, 3.5, 4.6 yr) (Fig. 5A and 5B) that coincide with the ENSO cycle (2–7 yr) (Li et al., 2011b; Liu et al., 2017).

Similarly, by the integration of the PCA method, we found that the first principal component of $\delta^{18}O_s$ variance can explain 43% of the stalagmite variability (Supplementary Figure S1) over the last millennium. Compared with the first principal component, 81% of the stalagmite variability can be explained from the first-three principal components (Fig. 4C). Due to $\delta^{18}O_s$ could be influenced by a combination of multiple factors, such as water vapor source, rainfall amount, and upstream convections, the first-three principal components are extracted for the main characteristics of the stalagmite variability in AAM region over the last millennium. According to our wavelet and power spectrum analysis results, there are significant multi-decadal to centennial periods (17, 28.6, 52.7, and 143 yr) (Fig. 5C and 5D), which is coupling with reconstructed ENSO records (Buckley et al., 2010; Nelson et al., 2011), supporting the teleconnection between AAM $\delta^{18}O_s$ and ENSO.

As mentioned above, the significant correlation between $\delta^{18}O_{aw}/\delta^{18}O_s$ and the SOI supports our proposal of linking $\delta^{18}O_s$ records to the ENSO variation over the past millennium in the AAM region (Figs. 2 and 4B). Applying this interpretation to $\delta^{18}O_s$ over the last millennium, we attribute the negative excursion in $\delta^{18}O$ in the Medieval Warm Period (MWP) to a more La Niña state. However, in the early stage of the LIA, the positive excursion of $\delta^{18}O_s$ coincided with more El Niño states, and the later stage of the LIA presented some obvious oscillations in the first-three principal components of AAM stalagmite records (Fig. 4C).

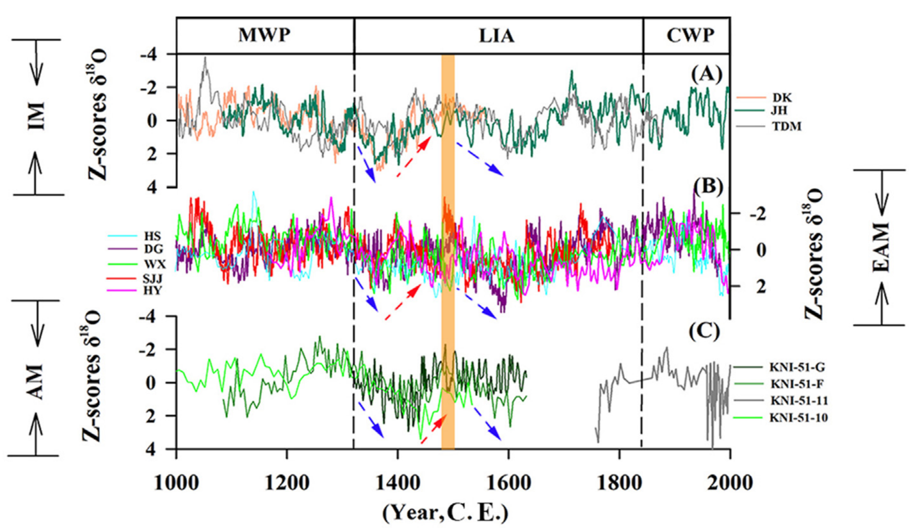

Fig. 3. Comparison of high-resolution stalagmite records in the AAM region after normalization to Z-scores. **(A)** Dandak (DK), Jhumar (JH) Cave and Tham Doun Mai (TDM) Cave stalagmite records in the IM region (Berkelhammer et al., 2010; Sinha et al., 2011; Wang et al., 2019). **(B)** Stalagmite records from the EAM region. Stalagmite WX record of Wanxiang Cave (Zhang et al., 2008); DG record from Dongge Cave (Zhao et al., 2015); HY record from Huangye Cave (Tan et al., 2011) HS record from Heshang Cave (Hu et al., 2008). The stalagmite SJJ record from Shijiangjun Cave (this study and Li et al., 2021). **(C)** Stalagmite records from KNI-51 Cave in the AM region (combined four stalagmites in the same cave, KNI-51-10, 11, F, G) (Denniston et al., 2016). MWP, LIA, and CWP indicate the Medieval Warm Period, Little Ice Age, and Current Warm Period, respectively. The red dashed arrows indicate the negative trend in the Z-scores of $\delta^{18}O_s$, and the blue dashed arrows indicate the positive trend in the Z-scores of $\delta^{18}O_s$. The dashed yellow columnar area is the peak isotopic value of all stalagmites during the LIA. (For interpretation of the references to colour in this figure legend, the reader is referred to the Web version of this article.)

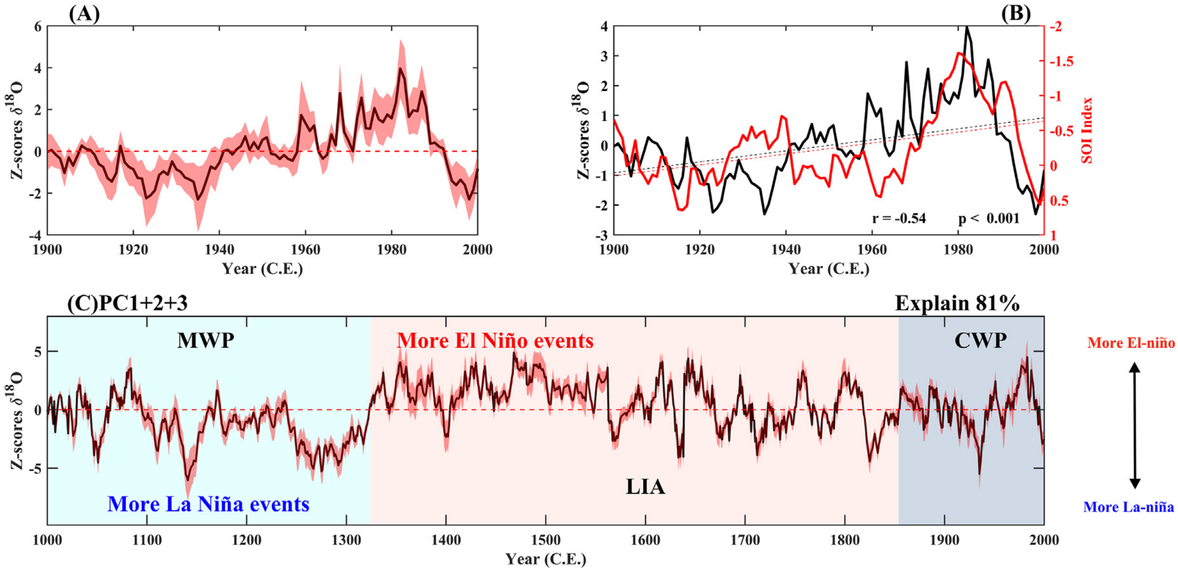

Fig. 4. **(A)** Principal component analysis (PCA) result for interannual trends in $\delta^{18}O_s$ over the past 100 years. **(B)** Validation test for the reconstructed ENSO index compared to the instrumental SOI in the period of 1900–2000 (C.E.). The red and black dashed lines are fitting trends. **(C)** The variability of the first, second, and third principal components explains 81% of the stalagmite $\delta^{18}O$ variability. We used the SOI data from the website (https://www.cgd.ucar.edu/cas/catalog/climind/SOI.signal.annstd.ascii) published by National Center for Atmospheric Research, USA. Because the resolution of stalagmites was usually on the multi-year and decadal scales, the original instrumental SOI index has been smoothed by 15 years to find the multi-year and decadal relationship between $\delta^{18}O_s$ and ENSO. (For interpretation of the references to colour in this figure legend, the reader is referred to the Web version of this article.)

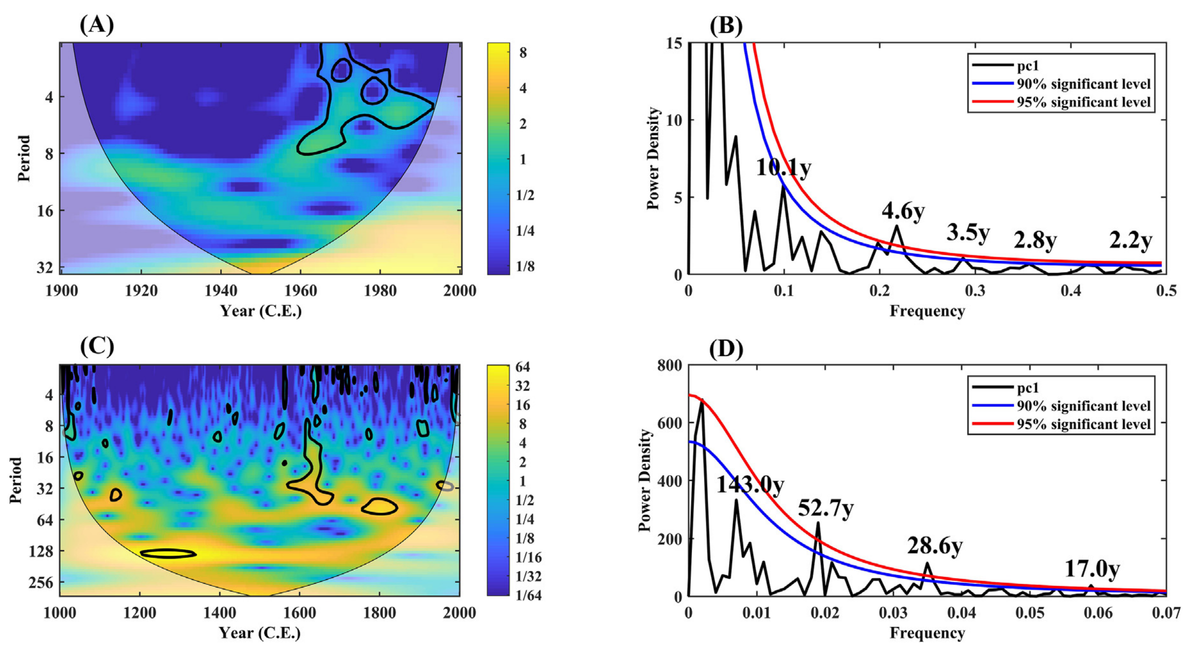

Fig. 5. **(A, B)** Wavelet and power spectrum analysis for the integrated $\delta^{18}O_s$ record of AAM stalagmites over the past 100 years show that there are significant ENSO periods. **(C, D)** Wavelet and power spectrum analysis for the integrated $\delta^{18}O_s$ record of AAM stalagmites over the past 1000 years.

5. Discussion

5.1. The main reasons for the change of $\delta^{18}O_p$ in the AAM region on a monthly-seasonal timescale

The negative correlation between $\delta^{18}O_p$ and monthly precipitation may be a mathematical relationship because the essence of isotope fractionation is a physical process during the transportation of moisture (Li, 2018). During the Rayleigh fractionation, more liquid water condenses from the air mass, depleting stable isotopic composition in the remaining water vapor, resulting in the lower $\delta^{18}O_{p.}$ Similarly, both the rapid condensation during convection (Dansgaard, 1964; Cai et al., 2017) and the "rain-out effect" (Rayleigh fractionation) of precipitation in the upstream air mass will lead to the depleted $\delta^{18}O_p$ in the down-stream air mass along with the transportation of moisture vapor (Breitenbach et al., 2010; Pausata et al., 2011; Li, 2018; Wang et al., 2020; Zhang et al., 2020).

The precipitation amount at each site in the AAM region may not

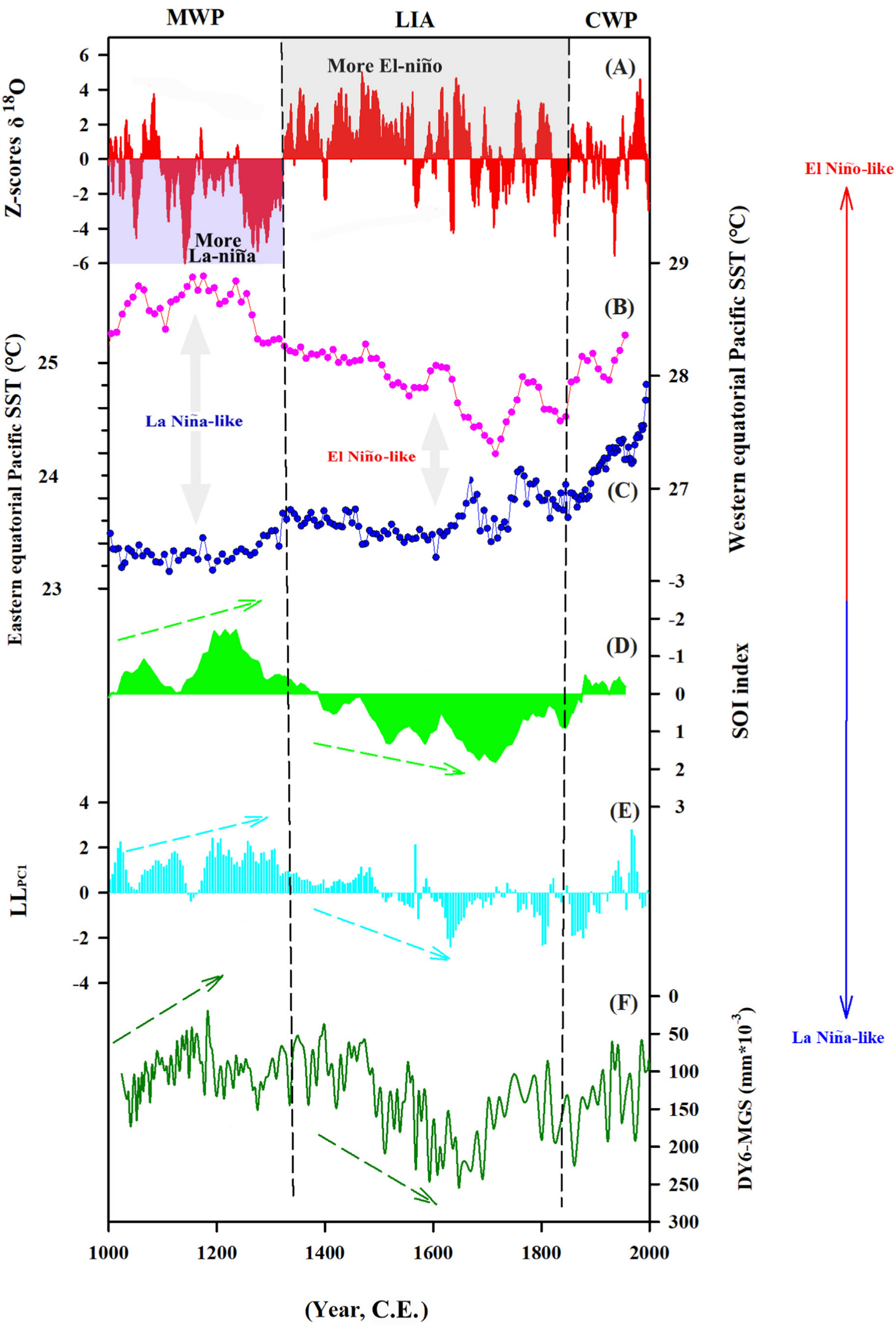

Fig. 6. Comparison of reconstructed ENSO variations and tropical Pacific hydrological records. **(A)** Stalagmite $\delta^{18}O$ Z-scores in the AAM region (this study). **(B)** Reconstructed SST of the western equatorial Pacific (Indo-Pacific Warm Pool) (Oppo et al., 2009). **(C)** SST reconstruction of the eastern equatorial Pacific (Conroy et al., 2009). **(D)** Reconstructed SOI based

be the direct factor dominating the change of $\delta^{18}O_p$. The evolution of atmospheric circulations and changes in moisture sources in different seasons were responsible for the change of $\delta^{18}O_p$ (Posmentier et al., 2004; Pausata et al., 2011; Zhang and Li, 2018; Li, 2018). Taking the EAM (East Asian Monsoon) region as an example, the water vapor during summer is mainly from tropical oceans (the Indian Ocean and the Pacific Ocean) (Ding and Chan, 2005; Chen and Li, 2018). With the multiple precipitations in the ocean-to-inland migration of moisture, water molecules of relatively more ^{18}O are preferentially dropped in the early stage of precipitation (i.e. “Rain-out effect”), resulting in relatively more ^{16}O in the remaining air mass and lower $\delta^{18}O$ in summer precipitation (Lee and Fung, 2008; Risi et al., 2008; Pausata et al., 2011; Kurita, 2013). Another evidence is that the $\delta^{18}O$ in summer precipitation (June-July-August) is notably negative than that in non-summer monsoon months (NSMM), even the amount of precipitation in some summer months is less than that in NSMM (Fig. 1 in Li, 2018).

In winter, for local precipitation in EAM, the proportion of continental water vapor increased compared to that during the summer months. The $\delta^{18}O$ of the continental water vapor is higher than the oceanic water vapor from tropical oceans, resulting in the higher $\delta^{18}O$ in winter precipitation. Besides, the atmospheric convection activity is weakened in winter, leading to the reduced air mass humidity and weakened Rayleigh fractionation, which makes the $\delta^{18}O_p$ more positively biased than that in the summer (Zhang and Li., 2019). In summary, the $\delta^{18}O_p$ values in the AAM region show a characteristic of “lower in the rainy season and higher in the dry season”, which is statistically negatively related to local monthly precipitation. While, the essential main reason is the difference in the source of water vapor in different seasons (Li, 2018).

5.2. The explanations for links between $\delta^{18}O_{aw}$/$\delta^{18}O_s$ variability and ENSO in the AAM region

A conceptual model is summarized in Supplementary Fig. S2, illustrating the potential mechanism of $\delta^{18}O_{aw}/\delta^{18}O_s$ variability in the AAM region. Statistically, interannual changes in $\delta^{18}O_p$ appear to be controlled by the “amount effect” in the IM region (Dansgaard, 1964), but there is no “amount effect” in the AM and EAM regions, which are affected by “composite moisture sources”. The significant correlation between the instrumental SOI and compositive Z-scores $\delta^{18}O_s$ have indicated a close linkage between ENSO and the variability of Asian-Australian monsoon (Figs. 2 and 4B).

In the IM region, El Niño circulation, in concert with tropical convection and Walker circulation, drives the ascending branch from the western Pacific to the east-central Pacific Ocean, creating a correlative anomalous sinking (atmospheric divergence) zone in the South-Asian subcontinent. Then, the downdraft airstream suppresses local convection, leading to a significant reduction in rainfall of the IM region (Supplementary Fig. S2A; Kumar et al., 1999; Zhang and Li, 2018). Consequently, $\delta^{18}O_{aw}$ and $\delta^{18}O_s$ in the IM region experience positive phases associated with the El Niño state due to the “amount effect” and “convective intensity” (Supplementary Fig. S2A).

Completely different from the IM region, the EAM and AM regions are subject to a composite water-vapor source (West Pacific and the Indian Ocean), so that $\delta^{18}O_{aw}$ and $\delta^{18}O_s$ may be dominated by the “circulation effect” characterized by the proximity of moisture transport pathway during El Niño states (Supplementary Fig. S2B; Tan et al., 2014). In this case, the “circulation effect” emphasizes the “rainout effect” during the transport of water vapor, governing variability in $\delta^{18}O_p$, whereas a decrease in transportation distances may result in higher $\delta^{18}O_{aw}$ and $\delta^{18}O_s$ values (Tan, 2014). However, some studies in the EAM region have suggested that upstream convection modulated by ENSO, rather than moisture source changes, affecting the change of interannual variation in $\delta^{18}O_p$ values based on $\delta^{18}O_p$ monitoring (Cai et al., 2017; Ruan et al., 2019). For example, Ruan et al. (2019) suggested that the primary moisture of southeastern China (Guangzhou) essentially comes from the proximal northern South China Sea, and convective activities over the primary moisture source regions played a key role in regulating $\delta^{18}O_p$ variability across different timescales (Ruan et al., 2019). We believe that the enhanced convective activity upstream of water vapor leads to increased precipitation in upstream and negative $\delta^{18}O_p$ in the downstream area, which is essentially equivalent to the “rainout effect".

ENSO events are fundamentally intertwined with the behavior of the Intertropical Convergence Zone (ITCZ) (Atwood and Sachs, 2014). The ITCZ is both a strong rainfall and a deep convective zone, and its changes reflect the change in the upstream convection intensity (Haug et al., 2001; Sachs et al., 2009; Eroglu et al., 2016). Dynamical theory may support the link between the location of the ITCZ and ENSO variability. Many studies have shown that the mean state of the tropical Pacific is governed by northern hemisphere in winter/spring (summer/autumn) conditions when the ITCZ is located to the south (north) of its annual mean location, which was expected to favor a decrease (increase) in ENSO variability (Atwood and Sachs, 2014). Tang et al., (2015) also found that the intraseasonal variation in Nanjing (Eastern China) $\delta^{18}O_p$ in summer was linked to the moisture source location and rainout processes that affected by the changes in ITCZ intensity. (Tang et al., 2015). In addition, ITCZ can also modulate the AAM through the movement of the mean position or contraction and cause reverse or synchronous changes between hemispheres (Yan et al., 2015; Zhao et al., 2015). For example, Yan et al. (2015) proposed that the East Asian summer monsoon and the Australian summer monsoon synchronously retreated from the tropics during the LIA, which was attributed to the contraction of the ITCZ during the LIA (Yan et al., 2015).

5.3. Comparison between the $\delta^{18}O_s$ sequence and tropical pacific hydrology

We made a comparison between the integrated $\delta^{18}O_s$ sequence in the AAM region and SST reconstructions based on Mg/Ca and $\delta^{18}O$ data on the planktonic foraminifera from the Indo-Pacific Warm Pool (IPWP) (Oppo et al., 2009) and diatom and pollen abundances in Galápagos Islands in the Eastern Equatorial Pacific (EEP) (Conroy et al., 2009), respectively (Fig. 6A, 6B, 6C). Normalized $\delta^{18}O_s$ records display a negative excursion during the MWP in the AAM region (Fig. 6A), corresponding to an increase in zonal SST gradient in the tropical east-west Pacific, indicating a La Niña state in the tropical Pacific (Fig. 6B and 6C). However, conditions during the LIA are opposite to this, corresponding to the persistent El Niño state.

Although the above-mentioned $\delta^{18}O_s$ sequence is different from ENSO reconstructions based on precipitation records in the Pacific Ocean (Yan et al., 2011b, Fig. 6D), the Flores LL_{PC1} stalagmite record (Griffiths et al., 2016, Fig. 6E), and DY-6 lake sediment record from Xisha Island, South China Sea (Yan et al., 2011a, Fig. 6F) indicate an

on precipitation in the Pacific Ocean (Yan et al., 2011b). **(E)** Flores LLPC1 stalagmite record (original data have been processed by an un-rotated principal components analysis, referred to Griffith et al., 2016) in Liang Luar on the east Indonesian island. **(F)** Lake sediment mean grain size of Dongdao Island, South China Sea (Yan et al., 2011a). Noted that, in the MWP and LIA periods, different reconstructed ENSO variations exhibited an opposite trend. The dashed arrows indicate the changing trend of paleoclimate records. The zonal gradient of tropical Pacific SST was decreased in LIA compared with that in the MWP period (B and C).

El Niño state in the tropical Pacific during the MWP (Fig. 6D, 6E, 6F). The "Ocean Dynamic Thermostat (ODT)" model is used to interpret the SST reconstruction from the IPWP in MWP (Held et al., 2006; Conroy et al., 2009, 2010). The increases in SST in the IPWP responds to changes in solar radiation during the MWP (Oppo et al., 2009). However, in the EEP, the compensation flow for upward cooling increases, which suppresses the increase in SST (Held et al., 2006; Conroy et al., 2009, 2010). The increased zonal gradients of sea-surface temperature between EEP and IPWP lead to the tropical Pacific Ocean experiencing a La Nina-like state. However, the ODT model only focused on oceanic influences, discounting atmospheric effects. Yan et al. (2011b) used a Coupled General Circulation Model (CGCM) to explain the other possible mechanism for increased SST in the IPWP during the LIA. The CGCM model focused on atmospheric effects using a simplified ocean-atmosphere coupling scheme (Held and Soden, 2006). However, Oppo et al. (2009) also proposed a new explanation that an enhanced Asian winter monsoon during the LIA and a southward shift of the tropical convergence zone might also have led to the increased precipitation in the IPWP during the LIA (Oppo et al., 2009). Consequently, it is still uncertain whether the increased precipitation during the LIA in the IPWP is controlled by the change in ENSO mode.

For the LIA, the reconstruction of ENSO based on SST and precipitation proxies presented a significant discrepancy (Fig. 6B–6F) (Oppo et al., 2009; Conroy et al., 2009, 2010; Yan et al., 2011a, 2011b; Griffiths et al., 2016). The previous reconstruction of ENSO based on precipitation may only provide indirect evidence (Fig. 6C–6F). Our $\delta^{18}O_s$ sequence reconstruction is based on a new explanation (atmospheric circulation), which is essentially consistent with the original definition of ENSO based on changes in SST gradient (Fig. 6A–6C; Conroy et al., 2010) and robustly tested by modern instrumental observations (Fig. 4B). There are indeed some regional differences in $\delta^{18}O_s$ variability from the AAM region in the last millennium. For example, the $\delta^{18}O_s$ values increase in MWP and decrease in LIA from Buddha Cave (Paulsen et al., 2003), Dayu Cave (Tan et al., 2009), and Klong Cave (Tan et al., 2019). These inconsistencies may be attributed to geographic distribution, dating points (chronological accuracy), and record resolution. Our study does not deny these regional differences, however, we are more concerned with this large-scale consistency based on hemispheric scales.

6. Conclusions

The "circulation effect" related to the change of ENSO modality, combining the "rainout effect" to change the moisture source of precipitation, dominates the variation of $\delta^{18}O_p/\delta^{18}O_s$ in EAM and AM. However, $\delta^{18}O_p/\delta^{18}O_s$ in IM is modulated by the "amount effect" and "upstream convective intensity", revealed by a significant correlation between $\delta^{18}O_p/\delta^{18}O_s$ and SOI. The significant periodicities identified in the AAM $\delta^{18}O_s$ time series are similar to that of ENSO in the multi-year to decadal timescales, indicating that ENSO plausibly exerted the multi-year to decadal influence on the evolution of AAM over the last millennium. The circulation pattern reconstructed from $\delta^{18}O_s$ in the AAM region supports the published reconstructions from SST gradients, indicating a more La Niña-like state during the MWP and a more El Niño-like state during the early stage of the LIA. This study reconstructed the variation of ENSO based on modern instrumental data, improving the reliability of the reconstruction. The new prospect of this study is to provide robust evidence to support the "circulation effect", confirmed the "circulation effect"-based explanation of stalagmite $\delta^{18}O$ in the EAM and AM regimes, and revealed differences of ENSO based on different reconstruction proxies, which is meaningful not only for paleoclimate research, but also for modern climate research.

Data availability statement

Atmospheric precipitation $\delta^{18}O$ data from meteorological stations were obtained from the Global Networks of Isotopes in Precipitation monitoring website (GNIP: https://nucleus.iaea.org/wiser/index.aspx) and our observations (Table S3; Zhang and Li, 2018). Stalagmite geochemical and age-model data were obtained from the NOAA (National Oceanic and Atmospheric Administration) website (NOAA: https://www.ncei.noaa.gov/products/paleoclimatology) and are summarized for comparison and integration in Table S4.

Competing financial interests

The authors declare no competing financial interests.

Author contributions

Jian. Zhang and Ming-Qiang. Liang: Conceptualization, Data analysis, Data curation, Formal analysis, Writing - Review & editing. **Ting-Yong Li**: Project administration, Funding acquisition, Conceptualization, Review & editing. **Chao-Jun Chen**: Data curation, Formal analysis. **Jun-Yun Li**: Funding acquisition, Conceptualization.

Declaration of competing interest

The authors declare that they have no known competing financial interests or personal relationships that could have appeared to influence the work reported in this paper.

Acknowledgments

This research was supported by the National Natural Science Foundation of China (NSFC, No. 42172204; 42011530078), and the Fundamental Research Funds for the Central Universities, China (No. XDJK 2017A010 and No. XDJK 2020D005) and Yunnan Fundamental Research Projects (grant NO. 202101AS070070) to T.-Y Li and J.-Y Li the China Scholarship Council (CSC) to J. Zhang (201906990014), NSFC (No. 42172204) to J.-Y. Li. We thank George S. Burr and Jonathan L. Baker for the improvement of the English quality.Two anonymous reviewers are greatly appreciated for their constructive comments and suggestions to improve the quality of this paper.

Appendix A. Supplementary data

Supplementary data to this article can be found online at https://doi.org/10.1016/j.quascirev.2022.107420.

References

Abdi, H., Williams, L.J., 2010. Principal component analysis. Wiley interdisciplinary reviews: Comput. Stat. 2 (4), 433–459. https://doi.org/10.1002/wics.101.
Alexander, M.A., Vimont, D.J., Chang, P., Scott, J.D., 2010. The impact of extratropical atmospheric variability on ENSO: testing the seasonal footprinting mechanism using coupled model experiments. J. Clim. 23 (11), 2885–2901. https://doi.org/10.1175/2010JCLI3205.1.
Atwood, A.R., Sachs, J.P., 2014. Separating ITCZ- and ENSO-related rainfall changes in the Galapagos over the last 3 kyr using D/H ratios of multiple lipid biomarkers. Earth Planet Sci. Lett. 404, 408–419. https://doi.org/10.1016/j.epsl.2014.07.038.
Buckley, B.M., Anchukaitis, K.J., Penny, D., Fletcher, R., Cook, E.R., Sano, M., Nam, Le Canh, Wichienkeeo, A., Minh, T.T., Hong, T.M., 2010. Climate as a contributing factor in the demise of Angkor, Cambodia. P. Natl. Acad. Sci. USA. 107, 6748–6752. https://doi.org/10.1073/pnas.091.
Berkelhammer, M., Sinha, A., Mudelsee, M., Cheng, H., Edwards, R.L., Cannariato, K., 2010. Persistent multidecadal power of the Indian summer monsoon. Earth Planet Sci. Lett. 290 (1–2), 166–172. https://doi.org/10.1016/j.epsl.2009.12.017.

Breitenbach, S.F., Adkins, J.F., Meyer, H., Marwan, N., Kumar, K.K., Haug, G.H., 2010. Strong influence of water vapor source dynamics on stable isotopes in precipitation observed in Southern Meghalaya, NE India. Earth Planet Sci. Lett. 292 (1–2), 1–220. https://doi.org/10.1016/j.epsl.2010.01.038.
Bowen, G.J., Cai, Z.Y., Fiorella, R.P., Putman, A.L., 2019. Isotopes in the water cycle: regional-to global-scale patterns and applications. Annu. Rev. Earth Planet Sci. 47, 453–479. https://doi.org/10.1146/annurev-earth-053018-060220.
Cai, Z., Tian, L., Bowen, G.J., 2017. ENSO variability reflected in precipitation oxygen isotopes across the Asian Summer Monsoon region. Earth Planet Sci. Lett. 475, 25–33. https://doi.org/10.1016/j.epsl.2017.06.035.
Chen, C.J., Li, T.Y., 2018. Geochemical characteristics of cave drip water respond to ENSO based on a 6-year monitoring work in Yangkou cave, Southwest China. J. Hydrol 561, 896–907. https://doi.org/10.1016/j.jhydrol.2018.04.061.
Chen, J., Chen, F., Feng, S., Huang, W., Liu, J., Zhou, A., 2015. Hydroclimatic changes in China and surroundings during the medieval climate anomaly and little ice age: spatial patterns and possible mechanisms. Quat. Sci. Rev. 107, 98–111. https://doi.org/10.1016/j.quascirev.2014.10.012.
Cobb, K.M., Charles, C.D., Cheng, H., Edwards, R.L., 2003. El Niño/Southern Oscillation and tropical Pacific climate during the last millennium. Nature 424 (6946), 271–276. https://doi.org/10.1038/nature01779.
Conroy, J.L., Restrepo, A., Overpeck, J.T., Steinitz-Kannan, M., Cole, J.E., Bush, M.B., Colinvaux, P.A., 2009. Unprecedented recent warming of surface temperatures in the eastern tropical Pacific Ocean. Nat. Geosci. 2, 46–50. https://doi.org/10.1038/ngeo390.
Conroy, J.L., Overpeck, J.T., Cole, J.E., 2010. El Niño/Southern Oscillation and changes in the zonal gradient of tropical Pacific Sea surface temperature over the last 1.2 ka. PAGES News 18, 32–34. https://doi.org/10.22498/pages.18.1.32.
Dansgaard, W., 1964. Stable isotopes in precipitation. Tellus 16 (4), 436–468. https://doi.org/10.1111/j.2153-3490.1964.tb00181.x.
Denniston, R.F., Asmerom, Y., Lachniet, M., Polyak, V.J., Hope, P., An, N., Rodzinyak, K., Humphreys, W.F., 2013. A last glacial maximum through middle Holocene stalagmite record of coastal Western Australia climate. Quat. Sci. Rev. 77, 101–112. https://doi.org/10.1016/j.quascirev.2013.07.002.
Denniston, R.F., Ummenhofer, C.C., Wanamaker, A.D., Lachniet, M.S., Villarini, G., Asmerom, Y., Polyak, V.J., Passaro, K.J., Cugley, J., Woods, D., Humphreys, W.F., 2016. Expansion and contraction of the Indo-Pacific tropical rain belt over the last three millennia. Sci. Rep. 6, 34485. https://doi.org/10.1038/srep34485.
Ding, Y.H., Chan, C.L., 2005. The East Asian summer monsoon: an overview. Meteorol. Atmos. Phys. 89, 117–142. https://doi.org/10.1007/s00703-005-0125-z.
Emile-Geay, J., Cobb, K.M., Mann, M.E., Wittenberg, A.T., 2013. Estimating central equatorial Pacific SST variability over the Past Millennium. Part I: methodology and validation. J. Clim. 26, 2302–2328. https://doi.org/10.1175/JCLI-D-11-00510.1.
Eroglu, D., McRobie, F.H., Ozken, I., Stemler, T., Wyrwoll, K.-H., Breitenbach, S.F.M., Marwan, N., Kurths, J., 2016. Seesaw relationship of the holocene East Asian Australian summer monsoon. Nat. Commun. 7, 12929. https://doi.org/10.1038/ncomms12929.
Gergis, J.L., Fowler, A.M., 2009. A history of ENSO events since A.D. 1525: implications for future climate change. Clim. Change 92, 343–387. https://doi.org/10.1007/s10584-008-9476-z.
Genty, D., Labuhn, I., Hoffmann, G., Danis, P.A., Mestre, O., Bourges, F., Wainer, K., Massault, M., Van Exter, S., Régnier, E., Orengo, Ph, Falourd, S., Minster, B., 2014. Rainfall and cave water isotopic relationships in two South-France sites. Geochem. Cosmochim. Acta 131 (5), 323–343. https://doi.org/10.1016/j.gca.2014.01.043.
Griffiths, M.L., Kimbrough, A.K., Gagan, M.K., Drysdale, R.N., Cole, J.E., Johnson, K.R., Zhao, J.X., Cook, B.I., Hellstrom, J.C., Hantoro, W.S., 2016. Western Pacific hydroclimate linked to global climate variability over the past two millennia. Nat. Commun. 7, 11719. https://doi.org/10.1038/ncomms11719.
Haug, G.H., Hughen, K.A., Sigman, D.M., Peterson, L.C., Röhl, U., 2001. Southward migration of the intertropical convergence zone through the Holocene. Science 293 (5533), 1304–1308. https://doi.org/10.1126/science.1059725.
Held, I.M., Soden, B.J., 2006. Robust responses of the hydrological cycle to global warming. J. Clim. 19 (21), 5686–5699. https://doi.org/10.1175/JCLI3990.1.
Hu, C.Y., Henderson, G.M., Huang, J.F., Xie, S.C., Sun, Y., Johnson, K.R., 2008. Quantification of Holocene Asian monsoon rainfall from spatially separated cave records. Earth Planet Sci. Lett. 266 (3–4), 221–232. https://doi.org/10.1016/j.epsl.2007.10.015.
Kumar, K.K., Rajagopalan, B., Cane, M.A., 1999. On the weakening relationship between the Indian monsoon and ENSO. Science 284 (5423), 2156–2159. https://doi.org/10.1126/science.284.5423.2156.
Kurita, N., 2013. Water isotopic variability in response to meso-scale convective system over the tropical ocean. J. Geophys. Res. Atmos. 118, 10376–10390. https://doi.org/10.1002/jgrd.50754.
Lachniet, M.S., 2009. Climatic and environmental controls on speleothem oxygen-isotope values. Quat. Sci. Rev. 28 (5–6), 412–432. https://doi.org/10.1016/j.quascirev.2008.10.021.
Lee, J.E., Fung, I., 2008. Amount effect" of water isotopes and quantitative analysis of post-condensation processes. Hydrol. Process. 22 (1), 1–8. https://doi.org/10.1002/hyp.6637.
Li, T.Y., 2018. False amount effect—a discussion on one issue of isotopic climatology. Quat. Sci. 38 (6), 1545–1548. https://doi.org/10.11928/j.issn.1001-7410.2018.06.20 (In Chinese).
Li, T.-Y., Xiao, S.-Y., Shen, C.-C., Zhang, J., Chen, C.-J., Cheng, H., Spötl, C., Huang, R., Wang, T., Li, J.-Y., Wu, Y., Liu, Z.-Q., Edwards, R., Yu, T.-L., 2021. Little Ice Age climate changes in Southwest China from a stalagmite $\delta^{18}O$ record. Palaeogeogr. Palaeoclimatol. Palaeoecol. 562, 110167. https://doi.org/10.1016/j.palaeo.2020.110167.
Li, T.-Y., Shen, C.-C., Li, H.-C., Li, J.-Y., Chiang, H.-W., Song, S.-Y., Yuan, D.-X., Lin, C.D.-J., Gao, P., Zhou, J., Wang, J.-L., Ye, M.-Y., Tang, L.-L., Xie, S.-Y., 2011a. Oxygen and carbon isotopic systematics of aragonite speleothems and water in Furong Cave, Chongqing, China. Geochem. Cosmochim. Acta 75, 4140–4156. https://doi.org/10.1016/j.gca.2011.04.003.
Li, J., Xie, S., Cook, E.R., Huang, G., D'Arrigo, R., Liu, F., Ma, J., Zheng, X., 2011b. Interdecadal modulation of El Nino amplitude during the past millennium. Nat. Clim. Change 1, 114–118. https://doi.org/10.1175/JCLI-D-12-00415.1.
Liu, J., Fu, G., Song, X., Charles, S.P., Zhang, Y., Han, D., Wang, S., 2010. Stable isotopic compositions in Australian precipitation. J. Geophys. Res. 115, D23307. https://doi.org/10.1029/2010JD014403.
Liu, Z., Alexander, M., 2007. Atmospheric bridge, oceanic tunnel, and global climatic teleconnections. Rev. Geophys. 45 (2), RG2005. https://doi.org/10.1029/2005RG000172.
Liu, Z.Y., Wen, X.Y., Brady, E.C., Otto-Bliesner, B., Yu, G., Lu, H.Y., Cheng, H., Wang, Y.J., Zheng, W.P., Ding, Y.H., Edwards, R.L., Cheng, J., Liu, W., Yang, H., 2014. Chinese cave records and the east Asia summer monsoon. Quat. Sci. Rev. 83, 115–128. https://doi.org/10.1016/j.quascirev.2013.10.021.
Liu, Y., Cobb, K.M., Song, H., Li, Q., Li, C.Y., Nakatsuka, T., An, Z., Zhou, W., Cai, Q., Li, J., Leavitt, S.W., Sun, C., Mei, R., Shen, C.C., Chan, M.H., Sun, J., Yan, L., Lei, Y., Ma, Y., Li, X., Chen, D., Linderholm, H.W., 2017. Recent enhancement of central Pacific El Nino variability relative to last eight centuries. Nat. Commun. 8, 15386. https://doi.org/10.1038/ncomms15386.
Mann, M.E., Cane, M.A., Zebiak, S.E., Clement, A., 2005. Volcanic and solar forcing of the tropical Pacific over the past 1000 years. J. Clim. 18, 447–456. https://doi.org/10.1175/JCLI-3276.1.
Mann, M.E., Bradley, R.S., Hughes, M.K., 2000. Long-term variability in the El Niño/southern oscillation and associated teleconnections. In: Diaz, H.F., Markgraf, V. (Eds.), El Niño and the Southern Oscillation—Multiscale Variability and Global and Regional Impacts. Cambridge Univ. Press, New York, pp. 357–412. https://doi.org/10.1017/CBO9780511573125.011.
McGregor, S., Timmernamm, A., Timm, O., 2010. A unified proxy for ENSO and PDO variability since 1650. Clim. Past 6 (1), 1–17. https://doi.org/10.5194/cp-6-1-2010.
Nelson, D.B., Abbott, M.B., Steinman, B., Polissar, P.J., Stansell, N.D., Ortiz, J.D., Rosenmeier, M.F., Finney, B.P., Riedel, J., 2011. Drought variability in the Pacific Northwest from a 6,000-yr lake sediment record. Proc. Natl. Acad. Sci. U.S.A. 108, 3870–3875. https://doi.org/10.1073/pnas.1.
Oppo, D.W., Rosenthal, Y., Linsley, B.K., 2009. 2,000-year-long temperature and hydrology reconstructions from the Indo-Pacific warm pool. Nature 460 (7259), 1113–1116. https://doi.org/10.1038/nature08233.
Pape, J.R., Banner, J.L., Mack, L.E., Musgrove, M., Guilfoyle, A., 2010. Controls on oxygen isotope variability in precipitation and cave drip waters, central Texas, USA. J. Hydrol. 385 (1–4), 203–215. https://doi.org/10.1016/j.jhydrol.2010.02.021.
Pausata, F., Battisti, D.S., Nisancioglu, K.H., Bitz, C.M., 2011. Chinese stalagmite $\delta^{18}O$ controlled by changes in the Indian monsoon during a simulated Heinrich event. Nat. Geosci. 4 (7), 474–480. https://doi.org/10.1038/ngeo1169.
Paulsen, D.E., Li, H.C., Ku, T.L., 2003. Climate variability in central China over the last 1270 years revealed by high-resolution stalagmite records. Quat. Sci. Rev. 22 (5–7), 691–701. https://doi.org/10.1016/S0277-3791(02)00240-8.
Pathak, A., Ghosh, S., Martinez, J.A., Dominguez, F., Kumar, P., 2017. Role of oceanic and land moisture sources and transport in the seasonal and interannual variability of summer monsoon in India. J. Clim. 30 (5), 1839–1859. https://doi.org/10.1175/JCLI-D-16-0156.1.
Posmentier, E.S., Feng, X., Zhao, M., 2004. Seasonal variations of precipitation $\delta^{18}O$ in eastern Asia. J. Geophys. Res. Atmos. 109 (D23). https://doi.org/10.1029/2004JD004510.
Rayleigh, J.W.S., 1896. Theoretical considerations respecting the separation of gases by diffusion and similar processes. Philos. Mag. A 42, 493–498. https://doi.org/10.1080/14786449608620944.
Ruan, J., Zhang, H., Cai, Z., Yang, X., Yin, J., 2019. Regional controls on daily to interannual variations of precipitation isotope ratios in Southeast China: implications for paleomonsoon reconstruction. Earth Planet Sci. Lett. 527, 115794. https://doi.org/10.1016/j.epsl.2019.115794.
Risi, C., Bony, S., Françoise, V., 2008. Influence of convective processes on the isotopic composition (δD and $\delta^{18}O$) of precipitation and water vapor in the tropics: 2. Physical interpretation of the amount effect. J. Geophys. Res. Atmos. 113, D19306. https://doi.org/10.1029/2008JD009943.
Ropelewski, C.F., Jones, P.D., 1987. An extension of the Tahiti-Darwin southern oscillation index. Mon. Weather Rev. 115, 2161–2165.
Sachs, J.P., Sachse, D., Smittenberg, R.H., Zhang, Z., Battisti, D.S., Golubic, S., 2009. Southward movement of the Pacific intertropical convergence zone AD 1400–1850. Nat. Geosci. 2 (7), 519–525. https://doi.org/10.1038/ngeo554.
Sinha, A., Cannariato, K.G., Stott, L.D., Cheng, H., Edwards, R.L., Yadava, M.G., Ramesh, R., Singh, I.B., 2007. A 900-year (600 to 1500 AD) record of the Indian summer monsoon precipitation from the core monsoon zone of India. Geophys. Res. Lett. 34, L16707. https://doi.org/10.1029/2007GL030431.
Sun, Z., Yang, Y., Zhao, J.Y., Tian, N., Feng, X.X., 2018. Potential ENSO effects on the oxygen isotope composition of modern speleothems: observations from Jiguan Cave, central China. J. Hydrol. 566, 164–174. https://doi.org/10.1016/

j.jhydrol.2018.09.015.
Tan, M., 2014. Circulation effect: response of precipitation $\delta^{18}O$ to the ENSO cycle in monsoon regions of China. Clim. Dynam. 42 (3–4), 1067–1077. https://doi.org/10.1007/s00382-013-1732-x.
Tan, M., 2016. Circulation background of climate patterns in the past millennium: uncertainty analysis and re-reconstruction of ENSO-like state. Sci. China Earth Sci. 59 (6), 1225–1241. https://doi.org/10.1007/s11430-015-5256-6.
Tan, L., Cai, Y., An, Z., Edwards, R.L., Cheng, H., Shen, C.C., Zhang, H., 2011. Centennial-to decadal-scale monsoon precipitation variability in the semi-humid region, northern China during the last 1860 years: records from stalagmites in Huangye Cave. Holocene 21 (2), 287–296. https://doi.org/10.1177/0959683610378880.
Tan, L., Shen, C.-C., Lowemark, L., Chawchai, S., Edwards, R.L., Cai, Y., Sebastian, F.M.B., Cheng, H., Chou, Y.-C., Duerrast, Helmut, Partin, J.W., Cai, W., Chabangborn, A., Gao, Y., Kwiecien, O., Wu, C.-C., Shi, Z., Hsu, H.H., Wohlfarth, B., 2019. Rainfall variations in central Indo-Pacific over the past 2,700 y. Proc. Natl. Acad. Sci. USA 019A 116 (35), 17201–17206.
Tan, L., Cai, Y., Cheng, H., An, Z., Edwards, R.L., 2009. Summer monsoon precipitation variations in central China over the past 750 years derived from a high-resolution absolute-dated stalagmite. Palaeogeogr. Palaeoclimatol. Palaeoecol. 280 (3–4), 432–439. https://doi.org/10.1016/j.palaeo.2009.06.030.
Tang, Y., Pang, H., Zhang, W., Li, Y., Wu, S., Hou, S., 2015. Effects of changes in moisture source and the upstream rainout on stable isotopes in precipitation—a case study in Nanjing, eastern China. Hydrol. Earth Syst. Sci. 19 (10), 4293–4306. https://doi.org/10.5194/hess-19-4293-2015.
Trenberth, K.E., 1997. The definition of El Niño. Bull. Am. Meteorol. Soc. 78 (12), 2771–2778.
Wang, B., Clemens, S.C., Liu, P., 2003. Contrasting the Indian and East Asian monsoons: implications on geologic timescales. Mar. Geol. 201 (1), 5–21. https://doi.org/10.1016/S0025-3227(03)00196-8.
Wang, Y., Hu, C., Ruan, J., Johnson, K.R., 2020. East Asian precipitation $\delta^{18}O$ relationship with various monsoon indices. J. Geophys. Res. Atmos. 125 (13), e2019JD032282. https://doi.org/10.1029/2019JD032282.
Wang, J.K., Johnson, K.R., Borsato, A., Amaya, D.J., Griffiths, M.L., Henderson, G.M., Frisia, S., Mason, A., 2019. Hydroclimatic variability in Southeast Asia over the past two millennia. Earth Planet Sci. Lett. 525, 115737. https://doi.org/10.1016/j.epsl.2019.115737.
Yan, H., Sun, L., Wang, Y., Huang, W., Qiu, S., Yang, C., 2011a. A record of the Southern Oscillation Index for the past 2,000 years from precipitation proxies. Nat. Geosci. 4 (9), 611–614. https://doi.org/10.1038/ngeo1231.
Yan, H., Sun, L.G., Oppo, D.W., Wang, Y.H., Liu, Z.H., Xie, Z.Q., Liu, X.D., Cheng, W.H., 2011b. South China Sea hydrological changes and Pacific Walker Circulation variations over the last millennium. Nat. Commun. 2, 293. https://doi.org/10.1038/ncomms1297.
Yan, H., Wei, W., Soon, W., An, Z., Zhou, W., Liu, Z., 2015. Dynamics of the intertropical convergence zone over the western Pacific during the little ice age. Nat. Geosci. 8, 315–320.
Zhang, J., Li, T.Y., 2018. Amount effect" vs. “Circulation effect": the climate significance of precipitation and stalagmite $\delta^{18}O$ in the Asian-Australian monsoon region over the past 1 ka. Quat. Sci. 38 (6), 1532–1544. https://doi.org/10.11928/j.issn.1001-7410.2018.06.19 (In Chinese).
Zhang, J., Li, T.-Y., 2019. Seasonal and inter-annual variation of hydro-chemical characteristics and stable isotopic compositions of drip waters in Furong Cave, Southwest China based on 12 years' monitoring. J. Hydrol. 572, 40–50. https://doi.org/10.1016/j.jhydrol.2019.02.052.
Zhang, J., Genty, D., Sirieix, C., Michel, S., Minster, B., Regnier, E., 2020. Quantitative assessment of moisture source and temperature governing rainfall $\delta^{18}O$ from 20 years long monitoring records in SW-France: importance for isotopic-based climate reconstructions. J. Hydrol. 591, 1–20.
Zhang, P., Cheng, H., Edwards, R.L., Chen, F., Wang, Y., Yang, X., Liu, J., Tan, M., Wang, X., Liu, J., An, C., Dai, Z., Zhou, J., Zhang, D., Jia, J., Jin, L., Johnson, K.R., 2008. A test of climate, sun, and culture relationships from an 1810-year Chinese cave record. Science 322, 940–942. https://doi.org/10.1126/science.1163965.
Zhao, K., Wang, Y., Edwards, R.L., Cheng, H., Liu, D., Kong, X., 2015. A high-resolved record of the Asian summer monsoon from Dongge cave, China for the past 1200 years. Quat. Sci. Rev. 122, 250–257. https://doi.org/10.1016/j.quascirev.2015.05.030.